

Heavy-fermion metals with hybridization nodes: Unconventional Fermi liquids and competing phases

Heidrun Weber and Matthias Vojta

Institut für Theoretische Physik, Universität zu Köln, Zùlpicher Straße 77, 50937 Köln, Germany

(Received 24 October 2007; revised manuscript received 25 January 2008; published 13 March 2008)

Microscopic models for heavy-fermion materials often assume a local, i.e., momentum-independent, hybridization between the conduction band and the local-moment f electrons. Motivated by recent experiments, we consider situations where this neglect of momentum dependence is inappropriate, namely, when the hybridization function has nodes in momentum space. We explore the thermodynamic and optical properties of the highly anisotropic heavy Fermi liquid, resulting from Kondo screening in a higher angular-momentum channel. The dichotomy in momentum space has interesting consequences: while, e.g., the low-temperature specific heat is dominated by heavy quasiparticles, the electrical conductivity at intermediate temperatures is carried by unhybridized light electrons. We then discuss aspects of the competition between Kondo effect and ordering phenomena induced by intermoment exchange. We propose that the strong momentum-space anisotropy plays a vital role in selecting competing phases. Explicit results are obtained for the interplay of unconventional hybridization with unconventional, magnetically mediated, superconductivity, utilizing variants of large- N mean-field theory. We make connections to recent experiments on CeCoIn_5 and other heavy-fermion materials.

DOI: [10.1103/PhysRevB.77.125118](https://doi.org/10.1103/PhysRevB.77.125118)

PACS number(s): 75.20.Hr, 75.30.Mb, 71.10.Li

I. INTRODUCTION

Recent years have seen a revival of research in heavy-fermion metals, due to the wealth of fascinating phenomena which can be found in these materials.^{1–5} These include non-trivial charge and spin order, unconventional superconductivity, non-Fermi-liquid behavior, as well as quantum criticality beyond the Landau–Ginzburg–Wilson paradigm. The standard microscopic description of heavy-fermion systems is based on versions of the Anderson or Kondo lattice models, consisting of conduction (c) electrons and local moments on a regular lattice, with a spatially local hybridization or Kondo coupling between c electrons and local moments. The formation of a heavy Fermi liquid in such a model originates from the screening of the local moments at low temperatures through a lattice generalization of the Kondo effect—this is reasonably well understood, e.g., using slave-particle or dynamical mean-field approaches.

For some materials, recent experiments^{6,7} indicate that the assumption of a local (i.e., momentum-independent) hybridization is insufficient for a full understanding of the data. For example, optical-conductivity measurements⁷ in CeMIn_5 ($M = \text{Co, Ir, Rh}$) do not show the conventional, frequently observed hybridization gap^{8–12} but instead have been interpreted in terms of a distribution of gap values. Microscopically, a momentum dependence in the hybridization is not surprising, as the local-moment orbitals are usually of f type and may hybridize with several conduction-electron orbitals. While in certain cases this momentum dependence does not lead to significant changes in observable properties (as compared to a local hybridization), the physics can be qualitatively different if the hybridization has zeros (i.e., nodes) in momentum space. In analogy with unconventional superconductors, having a pair wave function with nonzero internal angular momentum, we may call heavy-fermion materials “unconventional” Fermi liquids if the Kondo electron-hole pairs have nonzero angular momentum. Such unconventional

heavy Fermi liquids, formed below the coherence temperature in the described setting, will have, e.g., quasiparticles with strong momentum-space anisotropy, to be discussed in more detail in this paper. (It is worth pointing out that the existence of hybridization nodes does *not* imply that parts of the local moments remain unscreened.)

Importantly, unconventional hybridization will influence the entire complex phase diagram of heavy-fermion compounds, where the lattice Kondo effect and various types of long-range order compete for the same electrons. Clearly, a strong momentum dependence of the hybridization may favor or disfavor certain ordering phenomena. For instance, a dichotomy in momentum space arising from anisotropic Kondo physics may determine which (unconventional) superconducting phase is realized at lowest temperatures.

On the theory side, hybridization with higher angular momentum has been discussed in a few papers only. References 13 and 14 studied the case of a half-filled conduction where a Kondo semimetal replaces the conventional Kondo insulator—this physics is likely relevant to CeNiSn and CeRhSb .¹³ Recently, Ghaemi and Senthil¹⁵ examined aspects on “higher angular-momentum Kondo liquids,” starting from a Kondo lattice model with nonlocal Kondo coupling. Some of their results in the Fermi-liquid regime are related to ours below, and we shall comment on similarities and differences. Let us note that differentiation of electronic properties in momentum space is a common theme in correlated electron systems. For instance, in the copper oxide high-temperature superconductors, quasiparticle properties are known to vary strongly along the Fermi surface.¹⁶

The purpose of this paper is a detailed investigation of heavy-fermion metals featuring hybridization functions with momentum-space nodes. In the first part, we study important Fermi-liquid properties including Fermi surface, effective mass, specific heat, and optical conductivity. We also discuss the temperature-dependent electrical resistivity. The focus of the second part is on ordering phenomena competing with

Kondo screening. Here, we concentrate on magnetically mediated superconductivity. Assuming a direct exchange interaction between local moments, we discuss mean-field phase diagrams focusing on the interplay of hybridization symmetry and pairing symmetry. Most of the concrete calculations are done using the slave-boson mean-field approximation on two-dimensional lattices, but most of our ideas apply more generally, including to situations where the hybridization does not have nodes, but otherwise varies strongly in momentum space.

The remainder of the paper is organized as follows. In Sec. II, we introduce the microscopic model to be employed; its mean-field treatment is the subject of Sec. III. We shall point out the relation between Kondo and Anderson lattice models with nonlocal coupling between c and f electrons. Section IV is devoted to properties in the Fermi-liquid regime, comparing local with nonlocal (unconventional) hybridization. In particular, the optical conductivity will be calculated and discussed in relation to experiments on the CeMIn_5 compounds.⁷ In Sec. V, we shall touch upon the low-temperature physics beyond the slave-boson approximation. Section VI discusses qualitative properties of the electrical resistivity, in particular, the perturbatively accessible temperature regime above the single-impurity Kondo temperature T_K . The competition of Kondo screening and superconducting pairing is the subject of Sec. VII. Two regimes will be distinguished, depending on whether the transition temperature T_c is comparable to or smaller than the Fermi-liquid coherence temperature T_{coh} . An outlook will conclude the paper.

II. MODEL

In this paper, we shall restrict our considerations to two-band models of heavy-electron materials, with simple tight-binding hopping of electrons. We shall generalize the Anderson and Kondo lattice models to the case of a nonlocal coupling between the conduction (c) and local (f) electrons, and discuss the relation between two models.

The Hamiltonian of the Anderson lattice model is given by

$$\begin{aligned} \mathcal{H}_{\text{ALM}} = & \sum_{\mathbf{k}\sigma} (\epsilon_{\mathbf{k}} - \mu) c_{\mathbf{k}\sigma}^\dagger c_{\mathbf{k}\sigma} + \sum_{\mathbf{k}\sigma} (\epsilon_f - \mu) f_{\mathbf{k}\sigma}^\dagger f_{\mathbf{k}\sigma} \\ & + \sum_{\mathbf{k}\sigma} V_{\mathbf{k}} (f_{\mathbf{k}\sigma}^\dagger c_{\mathbf{k}\sigma} + c_{\mathbf{k}\sigma}^\dagger f_{\mathbf{k}\sigma}) + U \sum_i n_{f,i}^\uparrow n_{f,i}^\downarrow, \end{aligned} \quad (1)$$

where $c_{\mathbf{k}\sigma}^\dagger$ ($f_{\mathbf{k}\sigma}^\dagger$) creates a conduction (f) electron with momentum \mathbf{k} , spin σ , and energy $\epsilon_{\mathbf{k}}$ (ϵ_f). f and c electrons are hybridized via the momentum-dependent hybridization $V_{\mathbf{k}}$. Finally, U is the on-site Coulomb repulsion of f electrons. The chemical potential μ influences the band fillings n_c and n_f of the c and f electrons, respectively. (Note that \mathcal{H}_{ALM} has the full translational invariance of the underlying lattice.)

While a full microscopic treatment of the f -electron lattice would require to consider the low-energy Kramers doublet state, e.g., of one f electron in an f^1 configuration of Ce in the presence of spin-orbit and crystal-field interactions, we shall proceed with the simplified model [Eq. (1)]. Hence, we

shall take the momentum dependence of $V_{\mathbf{k}}$ as a phenomenological input, noting that it is dictated by the lattice structure and the overlap of c and f orbitals. (In principle, the momentum dependence of $V_{\mathbf{k}}$ can be further renormalized by interaction effects, see Sec. V below.) The directional dependence of $V_{\mathbf{k}}$ as function of \mathbf{k}/k may be expanded into spherical harmonics. Conventionally, one neglects all nonzero angular-momentum components and assumes a local hybridization $V_{\mathbf{k}}=V$. This paper is concerned with situations where the zero angular-momentum component is small or vanishes, and hence the momentum dependence of $V_{\mathbf{k}}$ can no longer be ignored (because, e.g., $V_{\mathbf{k}}$ displays nodes in momentum space). It is convenient to decompose $V_{\mathbf{k}}=V\beta_{\mathbf{k}}$, where the form factor $\beta_{\mathbf{k}}$ is dimensionless and normalized to, e.g., $\sum_{\mathbf{k}}\beta_{\mathbf{k}}^2=\mathcal{N}$, where \mathcal{N} is the number of lattice sites. It is obvious that the thermodynamics as well as most other observables of the system will depend on $|V_{\mathbf{k}}|^2$ only; exceptions will be noted in the course of the paper. The f level is assumed to be nondispersive; this approximation is relaxed in Sec. VII.

In the Kondo limit, i.e., $V\rightarrow\infty$, $U\rightarrow\infty$, $\epsilon_f\rightarrow-\infty$ with V^2/ϵ_f finite, charge fluctuations are frozen. A Schrieffer–Wolff transformation,⁵ which projects out empty and doubly occupied states of the f levels, leads to a Kondo lattice model,

$$\mathcal{H}_{\text{KLM}} = \sum_{\mathbf{k}\sigma} \bar{\epsilon}_{\mathbf{k}} c_{\mathbf{k}\sigma}^\dagger c_{\mathbf{k}\sigma} + \underbrace{\sum_{\mathbf{k}\mathbf{k}'} 2J_{\mathbf{k}\mathbf{k}'} e^{-i(\mathbf{k}'-\mathbf{k})\mathbf{R}_i} \mathbf{S}_i \cdot \mathbf{s}_{\mathbf{k},\mathbf{k}'}}_{\mathcal{H}_J}, \quad (2)$$

where $\mathbf{s}_{\mathbf{k}\mathbf{k}'} = \sum_{\sigma\sigma'} c_{\mathbf{k}\sigma}^\dagger c_{\mathbf{k}\sigma} \sigma_{\sigma\sigma'} c_{\mathbf{k}'\sigma'}/2$ and $\bar{\epsilon}_{\mathbf{k}} = \epsilon_{\mathbf{k}} - \mu$. In the Kondo limit, n_f is fixed to unity, and \mathbf{S}_i is the local moment at site i formed out of the f electrons. (An additional potential scattering term arising from the Schrieffer–Wolff transformation will be neglected.) To leading order, the Kondo coupling is

$$J_{\mathbf{k}\mathbf{k}'} = 2V_{\mathbf{k}}V_{\mathbf{k}'} \left(\frac{1}{U + \epsilon_f} + \frac{1}{-\epsilon_f} \right) = J_0 \beta_{\mathbf{k}} \beta_{\mathbf{k}'}, \quad (3)$$

where $J_0 = V^2 \left(\frac{1}{U + \epsilon_f} + \frac{1}{-\epsilon_f} \right)$. In real space, the Kondo interaction \mathcal{H}_J takes the form

$$\mathcal{H}_J = 2J_0 \sum_{imn} \beta_{n-i} \beta_{m-i} \mathbf{S}_i \cdot \mathbf{s}_{mn}, \quad (4)$$

where β_{n-i} denotes the Fourier transform of $\beta_{\mathbf{k}}$ depending on the distance $|\mathbf{R}_n - \mathbf{R}_i|$ and $\mathbf{s}_{mn} = \sum_{\sigma\sigma'} c_{m\sigma}^\dagger \sigma_{\sigma\sigma'} c_{n\sigma'}/2$ is a *non-local* conduction-electron spin density.

Importantly, for each impurity \mathbf{S}_i , Eq. (4) describes a *single-channel* Kondo model, with the exchange “symmetry” determined by the hybridization symmetry of the underlying Anderson model. In contrast, Ghaemi and Senthil¹⁵ start out from a Kondo lattice model, where each local moment is exchange coupled to neighboring conduction-electron sites as follows:

$$\mathcal{H}'_J = 2 \sum_{im} J_{im} \mathbf{S}_i \cdot \mathbf{s}_{mm}. \quad (5)$$

This is a *multichannel* Kondo model, where the different screening channels correspond to different linear combina-

tions of the conduction electrons at the surrounding sites m . In such a model, the screening channels are of different strengths, and the strongest will dominate the low-temperature physics. The authors of Ref. 15 argue that, depending on microscopics (i.e., lattice and band structure properties), a higher-angular-momentum channel (e.g., d wave) can dominate over the conventional symmetric (s wave) channel. The general relation between Anderson and Kondo models with nonlocal coupling has been discussed, e.g., in Ref. 17. There, it was argued that, in an Anderson model, the coupling to a *correlated* conduction band opens new screening channels, and the effective model will be a multichannel Kondo model because the charge fluctuations in the band (accompanying the nonlocal hopping) are suppressed by conduction-electron correlations.

For our purpose, we note that the two Kondo lattice models with \mathcal{H}_J and \mathcal{H}'_J (with one screening channel dominating) become equivalent in the slave-boson mean-field (saddle-point) analysis employed below because the different screening channels correspond to different saddle points. Therefore, our mean-field results derived for the single-channel models [Eqs. (1) and (2)] can be directly compared with the ones for the multichannel Kondo model in Ref. 15.

III. MEAN-FIELD APPROXIMATION

To obtain quantitative results, we shall employ the standard slave-boson mean-field approximation for the Kondo and Anderson lattice models (the latter with infinite U). In the following, we briefly summarize the corresponding formalism.^{5,18,19} Note that in all cases, we restrict our attention to states with spatial translational invariance.

We start with the Anderson model. For infinite on-site repulsion, the three states of each f orbital can be represented by auxiliary fermions $\tilde{f}_{i\sigma}$ and spinless bosons r_i , such that the physical f electrons $f_{i\sigma} = r_i^\dagger \tilde{f}_{i\sigma}$, together with the constraint

$$\sum_{\sigma} \tilde{f}_{i\sigma}^\dagger \tilde{f}_{i\sigma} + r_i^\dagger r_i = 1. \quad (6)$$

At the saddle point, the slave bosons condense, $\langle r_i \rangle = r$, which implies a rigid hybridization between the c and the \tilde{f} bands. The mean-field Hamiltonian of the Anderson lattice model reads

$$\begin{aligned} \mathcal{H}_{\text{ALM,MF}} = & \sum_{\mathbf{k}\sigma} \epsilon_{\mathbf{k}} c_{\mathbf{k}\sigma}^\dagger c_{\mathbf{k}\sigma} + \sum_{\mathbf{k}\sigma} \epsilon_f \tilde{f}_{\mathbf{k}\sigma}^\dagger \tilde{f}_{\mathbf{k}\sigma} \\ & + \sum_{\mathbf{k}\sigma} V_{\mathbf{k}} r (\tilde{f}_{\mathbf{k}\sigma}^\dagger c_{\mathbf{k}\sigma} + c_{\mathbf{k}\sigma}^\dagger \tilde{f}_{\mathbf{k}\sigma}) \\ & - \lambda \left[\sum_{\mathbf{k}\sigma} \tilde{f}_{\mathbf{k}\sigma}^\dagger \tilde{f}_{\mathbf{k}\sigma} + \mathcal{N}(r^2 - 1) \right] \\ & - \mu \left[\sum_{\mathbf{k}\sigma} c_{\mathbf{k}\sigma}^\dagger c_{\mathbf{k}\sigma} - \mathcal{N}n_c \right], \end{aligned} \quad (7)$$

where λ is the Lagrange multiplier implementing the constraint [Eq. (6)] at the mean-field level, and the effect of the chemical potential μ on the \tilde{f} electrons has been absorbed in λ . The three mean-field parameters r , λ , and μ are obtained

from minimizing the free energy, leading to the self-consistency equations

$$\sum_{\mathbf{k}\sigma} V_{\mathbf{k}} \langle \tilde{f}_{\mathbf{k}\sigma}^\dagger c_{\mathbf{k}\sigma} + \text{H.c.} \rangle = 2\mathcal{N}\lambda r, \quad (8a)$$

$$\sum_{\mathbf{k}\sigma} \langle \tilde{f}_{\mathbf{k}\sigma}^\dagger \tilde{f}_{\mathbf{k}\sigma} \rangle = \mathcal{N}(1 - r^2), \quad (8b)$$

$$\sum_{\mathbf{k}\sigma} \langle c_{\mathbf{k}\sigma}^\dagger c_{\mathbf{k}\sigma} \rangle = \mathcal{N}n_c. \quad (8c)$$

The expectation values can be easily expressed in terms of the Green's function of the diagonalized mean-field Hamiltonian; for details, see Appendix A.

For the mean-field analysis of the Kondo lattice model, one represents the local moments \mathbf{S}_i by auxiliary fermions $\tilde{f}_{i\sigma}$, $\mathbf{S}_i = \frac{1}{2} \sum_{\sigma\sigma'} \tilde{f}_{i\sigma}^\dagger \sigma_{\sigma\sigma'} \tilde{f}_{i\sigma'}$, with the constraint

$$\sum_{\sigma} \tilde{f}_{i\sigma}^\dagger \tilde{f}_{i\sigma} = 1. \quad (9)$$

The Kondo interaction takes the form

$$\mathcal{H}_J = -J_0 \sum_{imn\sigma\sigma'} \beta_{n-i} \beta_{m-i} \tilde{f}_{i\sigma}^\dagger c_{n\sigma} c_{m\sigma'}^\dagger \tilde{f}_{i\sigma'}, \quad (10)$$

where additional bilinear terms have been dropped, as they can be absorbed in chemical potentials. The Kondo interaction term \mathcal{H}_J can be decoupled using auxiliary fields b_i conjugate to $(-J_0 \sum_{n\sigma} \beta_{n-i} \tilde{f}_{i\sigma}^\dagger c_{n\sigma})$, i.e., b_i reflects the hybridization between the \tilde{f} and c bands at site i . At the saddle point, the b_i condense, and translational invariance dictates $b_i = b$. The Kondo lattice mean-field Hamiltonian is

$$\begin{aligned} \mathcal{H}_{\text{KLM,MF}} = & \sum_{\mathbf{k}\sigma} \epsilon_{\mathbf{k}} c_{\mathbf{k}\sigma}^\dagger c_{\mathbf{k}\sigma} + b \sum_{\mathbf{k}\sigma} \beta_{\mathbf{k}} (c_{\mathbf{k}\sigma}^\dagger \tilde{f}_{\mathbf{k}\sigma} + \text{H.c.}) + \mathcal{N} \frac{b^2}{J_0} \\ & - \lambda_0 \left(\sum_{\mathbf{k}\sigma} \tilde{f}_{\mathbf{k}\sigma}^\dagger \tilde{f}_{\mathbf{k}\sigma} - \mathcal{N} \right) - \mu \left(\sum_{\mathbf{k}\sigma} c_{\mathbf{k}\sigma}^\dagger c_{\mathbf{k}\sigma} - \mathcal{N}n_c \right). \end{aligned} \quad (11)$$

As before, the three parameters b , λ_0 , and μ are determined by self-consistency equations, which now read

$$\sum_{\mathbf{k}\sigma} \beta_{\mathbf{k}} \langle \tilde{f}_{\mathbf{k}\sigma}^\dagger c_{\mathbf{k}\sigma} + \text{H.c.} \rangle = -\mathcal{N} \frac{2b}{J_0}, \quad (12a)$$

$$\sum_{\mathbf{k}\sigma} \langle \tilde{f}_{\mathbf{k}\sigma}^\dagger \tilde{f}_{\mathbf{k}\sigma} \rangle = \mathcal{N}, \quad (12b)$$

$$\sum_{\mathbf{k}\sigma} \langle c_{\mathbf{k}\sigma}^\dagger c_{\mathbf{k}\sigma} \rangle = \mathcal{N}n_c. \quad (12c)$$

These mean-field equations are equivalent to the ones of the Anderson lattice model [Eq. (8)] if the Kondo limit is taken there; for details, see Appendix B.

We note that mean-field Hamiltonians [Eqs. (7) and (11)] represent the $N = \infty$ saddle-point solutions of certain $\text{SU}(N)$ Anderson and Kondo lattice models. In this mean-field picture, both the Anderson and Kondo lattice models are

mapped onto two-band systems of noninteracting fermions with a self-consistently determined renormalized hybridization between the bands. At high temperature, the slave-boson condensation amplitude vanishes (leading to two decoupled bands), whereas the condensation amplitude is finite below the single-impurity Kondo temperature T_K . In the Kondo lattice model, T_K is given by

$$\frac{2}{J_0} = \frac{1}{\mathcal{N}} \sum_{\mathbf{k}} \frac{\beta_{\mathbf{k}}^2}{\bar{\epsilon}_{\mathbf{k}}} \tanh \frac{\bar{\epsilon}_{\mathbf{k}}}{2T_K}, \quad (13)$$

with $\bar{\epsilon}_{\mathbf{k}} = \epsilon_{\mathbf{k}} - \mu$. The neglect of fluctuations in the mean-field approach causes an artificial finite-temperature transition at T_K , which can, in principle, be cured by including the coupling to a U(1) gauge field, see Sec. V.

The effective two-band picture is appropriate to describe the low-temperature Fermi-liquid regime, i.e., the quasiparticle physics for temperatures below the Fermi-liquid coherence temperature T_{coh} . An approximation for T_{coh} can be extracted from the $T=0$ slave-boson solution. For the Kondo lattice model, one obtains $T_{\text{coh}} = b^2/D$, where D is the bandwidth.¹⁹ (Also, $\lambda_0 \propto T_{\text{coh}}$.) The Fermi surface resulting from the slave-boson approximation fulfills Luttinger's theorem: The momentum-space volume enclosed by the Fermi surface is proportional to the total number of electrons $n_{\text{tot}} = n_c + n_f$, where $n_f = 1$ in the Kondo limit. At small nonzero temperature T , the mean-field parameters acquire quadratic T corrections characteristic of a Fermi liquid, e.g., $[b(T) - b_0]/b_0 \propto -T^2/T_K^2$, where $b_0 = b(T=0)$.

The simple two-band picture of the slave-boson approach has been confirmed, e.g., using the dynamical mean-field theory²⁰ (DMFT) approach to the Anderson lattice model, which fully includes local correlations and inelastic processes. The DMFT results²¹ nicely show the formation of a coherent heavy band crossing the Fermi level at low temperatures, rather well separated from the second band.

IV. LOW-TEMPERATURE PROPERTIES OF THE FERMILIQUID STATE

This section will discuss the properties of the heavy-Fermi-liquid state in a heavy-fermion system with unconventional hybridization. Effects of intermoment exchange and possible ordered phases will be ignored; we will come back to these issues in Sec. VII. Quantitative results will be obtained by solving the slave-boson mean-field equations for different model parameters, but the qualitative aspects will be of general validity unless otherwise noted.

We restrict ourselves to two-dimensional systems on a square lattice. For the c electrons, a tight-binding dispersion will be assumed,

$$\epsilon_{\mathbf{k}} = -2t(\cos k_x + \cos k_y). \quad (14)$$

Results will be shown for hybridization functions of the form $V_{\mathbf{k}} = V_0 \beta_{\mathbf{k}}$ with

$$\beta_{\mathbf{k}} = \begin{cases} 1 & s \text{ wave} \\ \cos k_x + \cos k_y & \text{extended } s \text{ wave} \\ \cos k_x - \cos k_y & d_{x^2-y^2} \text{ wave.} \end{cases} \quad (15)$$

The $d_{x^2-y^2}$ -wave and the extended s -wave case correspond to different linear combinations of hybridization between an f site and its nearest-neighbor c sites (also discussed by Ghaemi and Senthil¹⁵), while the s -wave case with local hybridization is shown for comparison.

In addition, we will also consider a lattice appropriate to model the CeIn planes of the CeMIn₅ materials ($M = \text{Ir, Rh, Co}$). Those crystallize in a HoCoGa₅-type tetragonal structure,^{22,23} where the Ce and the in-plane In ions are located on two interpenetrating square lattices. Thus, we assume a c -electron dispersion as in Eq. (14) and hybridization functions of the form

$$\beta_{\mathbf{k}} = \begin{cases} 2 \cos \frac{k_x}{2} \cos \frac{k_y}{2} & \text{extended } S \text{ wave} \\ 2 \sin \frac{k_x}{2} \sin \frac{k_y}{2} & D_{xy} \text{ wave.} \end{cases} \quad (16)$$

Hybridization functions $\beta_{\mathbf{k}}$ which formally break inversion symmetry, i.e., have odd angular momentum l , are possible as well. Observables are governed by $V_{\mathbf{k}}^2$ and display inversion symmetry; hence, there is little qualitative difference between even and odd angular-momentum hybridization (apart from the location of the hybridization nodes). Exceptions are transport anisotropies for $l=1$, briefly discussed in Sec. IV E.

A. Band structure and Fermi surface

To simplify the discussion, we shall work in the Kondo limit. The eigenvalues of the mean-field Hamiltonian [Eq. (11)], representing the effective bands of the heavy Fermi liquid, are given by

$$z_{1,2\mathbf{k}} = \frac{1}{2} [-\lambda_0 + \bar{\epsilon}_{\mathbf{k}} \pm \sqrt{(\lambda_0 + \bar{\epsilon}_{\mathbf{k}})^2 + 4b^2\beta_{\mathbf{k}}^2}]. \quad (17)$$

This band structure is illustrated in Fig. 1. Along certain ‘‘nodal’’ lines in momentum space, the hybridization vanishes, and the two bare bands of the c and \tilde{f} particles cross [Fig. 1(a)]; for $d_{x^2-y^2}$ symmetry, this applies to $k_x = \pm k_y$. Otherwise, the hybridization causes a band repulsion [Fig. 1(b)], which is maximum in the ‘‘antinodal’’ direction. As the bare \tilde{f} band is nondispersive, the two bands $z_{1,2\mathbf{k}}$ do not overlap, and consequently only one band crosses the Fermi level. For less than half filling, $n_c < 1$, the Fermi surface is thus determined by $z_{2\mathbf{k}} = 0$.

Figure 1 also shows the momentum distribution function of the c electrons, $n_{\mathbf{k}} = \langle c_{\mathbf{k}}^\dagger c_{\mathbf{k}} \rangle$. It shows a jump at the Fermi wave vector k_F , the jump height given by the quasiparticle weight Z , see below. As typical for heavy-fermion systems, $n_{\mathbf{k}}$ also shows a rounded step at the ‘‘small’’ Fermi surface of the original c electrons, i.e., the Fermi surface in the absence of a hybridization (or at temperatures $T \gg T_{\text{coh}}$).

Sample results from a full numerical solution of the mean-field equations [Eq. (12)] are shown in Figs. 2–5 be-

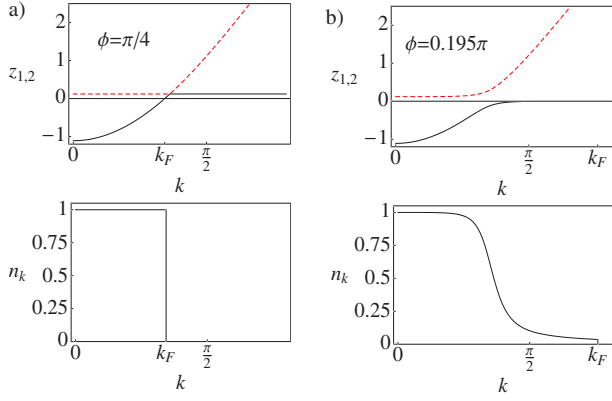


FIG. 1. (Color online) Dispersion relation of the two effective bands, $z_{1,2k}$ [Eq. (17)], and the corresponding momentum distribution function $n_{\mathbf{k}}$, for a $d_{x^2-y^2}$ -wave hybridization on a 2D square lattice, (a) along the momentum-space diagonal and (b) along a direction which encloses the angle 0.195π with the k_x axis. The parameters of the Kondo lattice model are $J_0/t=2.0$ and $n_c=0.4$.

low. Figure 2 displays two-dimensional (2D) Fermi surfaces for the hybridization functions of Eq. (15), with parameters chosen such that the specific-heat coefficient is identical in the four cases, see below. For $d_{x^2-y^2}$ -wave hybridization [Figs. 2(c) and 2(d)], one clearly observes a small Fermi momentum k_F along the nodal directions, while k_F is “large” along the antinodal direction. Note that the function $k_F(\phi)$, where ϕ is the angle parametrizing the k -space direction, can be multivalued due to the momentum dependence of $V_{\mathbf{k}}$. Analyzing the equation $z_{2k}=0$, one finds that this generically happens for small band filling n_c [Fig. 2(d)]. In the case of extended s -wave hybridization [Fig. 2(b)], two Fermi sheets emerge, as the lower band crosses the Fermi level twice.

For the hybridizations of Eq. (16), arising from two interpenetrating square lattices of c and f electrons, sample Fermi surfaces are shown in Fig. 3. In the d -wave case [Fig. 3(b)], the nodal lines are simply rotated by 45° with respect to Figs. 2(c) and 2(d).

B. Thermodynamic properties

The leading low-temperature thermodynamics can be directly obtained from the effective two-band description of

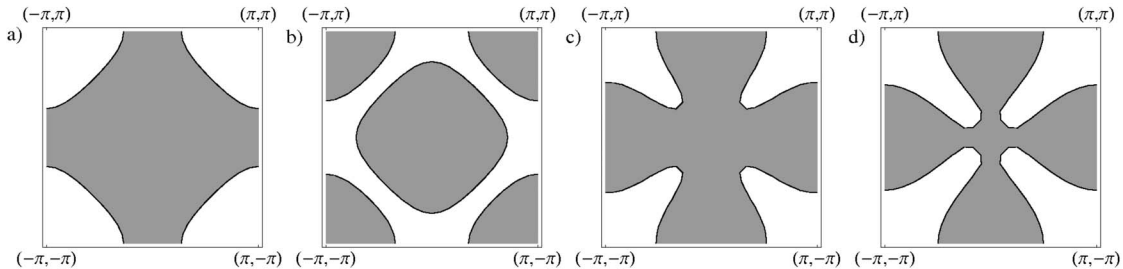


FIG. 2. Fermi surfaces for (a) s -wave, (b) extended s -wave, and [(c) and (d)] $d_{x^2-y^2}$ -wave hybridization. The band filling is $n_c=0.3$ in panels (a)–(c), whereas $n_c=0.1$ in panel (d); the Kondo coupling is chosen such that the specific-heat coefficient is identical in all four cases: (a) $J_0/t=1.0$ ($\lambda_0=-0.025$, $\mu=-2.47$, $b=0.281$), (b) $J_0/t=0.89$ ($\lambda_0=-0.0067$, $\mu=-2.3$, $b=0.281$), (c) $J_0/t=0.97$ ($\lambda_0=-0.0061$, $\mu=-2.46$, $b=0.173$), and (d) $J_0/t=1.957$ ($\lambda_0=-0.0385$, $\mu=-3.698$, $b=0.466$).

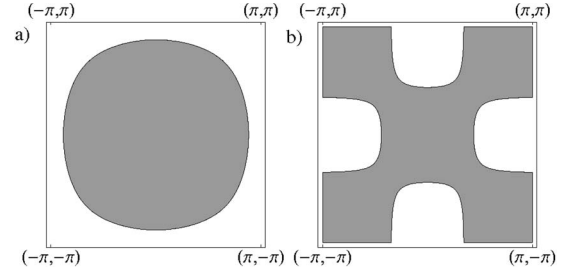


FIG. 3. Fermi surfaces using the hybridization functions [Eq. (16)] for interpenetrating c and f square lattices. (a) Extended s wave with $J_0/t=0.46$ ($\lambda_0/t=-0.011$, $\mu/t=-2.38$, $b/t=0.187$) and (b) d_{xy} -wave with $J_0/t=1.975$ ($\lambda_0/t=-0.001$, $\mu/t=-2.34$, $b/t=0.138$). In both cases, $n_c=0.3$, and the parameters are chosen such that the γ coefficient is the same as for the data in Fig. 2.

the slave-boson approximation.²⁴ For noninteracting fermions, the Sommerfeld coefficient, $\gamma=C_V/T$, of the specific heat is related to the density of states (per spin) at the Fermi level, $N_0=N(\omega=0)$, through $\gamma=\frac{2\pi^2}{3}N_0$. In standard isotropic Fermi-liquid theory, the effective mass m^* is defined through the slope of the dispersion at the Fermi level, $v_F=k_F/m^*$, where v_F and k_F are Fermi velocity and Fermi momentum, respectively. The density of states is $N_0=m^*k_F^{d-2}/C_d$ in d dimensions, where $C_2=2\pi$ and $C_3=2\pi^2$.

In anisotropic systems, a suitable definition for a (direction-dependent) effective mass is

$$\frac{1}{m^*(\mathbf{k})} = \frac{1}{k} \left| \frac{\partial \epsilon_{\mathbf{k}}}{\partial \mathbf{k}} \right|_{\text{FS}} \quad (18)$$

where $\epsilon_{\mathbf{k}}$ is the quasiparticle energy of the band crossing the Fermi surface (FS) and $k=|\mathbf{k}|$. Then, the density of states is given by

$$N_0 = \int_{\text{FS}} \frac{d^{d-1}k}{(2\pi)^d} \frac{m^*(\mathbf{k})}{k}. \quad (19)$$

Note that Ref. 15 defined a quantity m^* via the second (instead of the first) derivative of quasiparticle energies, which, in general, plays only a subleading role in thermodynamics.

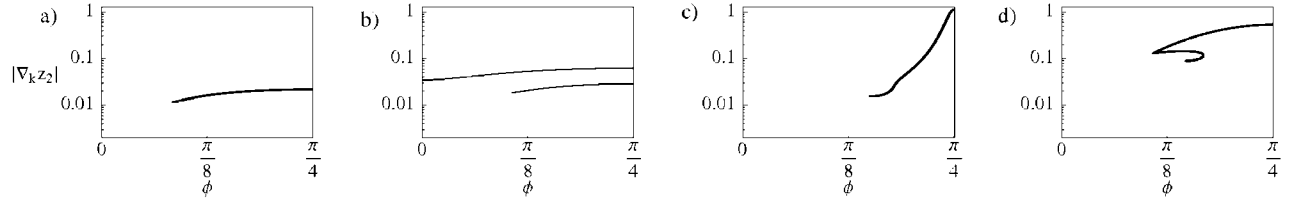


FIG. 4. The quasiparticle velocity at the Fermi level, $|\nabla_{\mathbf{k}} z_{2\mathbf{k}}|$, in a logarithmic plot vs momentum-space angle ϕ for (a) s -wave, (b) extended s -wave, and [(c) and (d)] $d_{x^2-y^2}$ -wave hybridization. Parameters are as in Figs. 2(a)–2(d). In all four cases, the “total” effective mass (as derived from the specific heat) is around 125 times the bare electron mass.

In our two-band system, $\epsilon_{\mathbf{k}} = z_{2\mathbf{k}}$ for $n_c < 1$. In $d=2$, some factors of k drop out, such that

$$N_0 = \frac{m^*}{2\pi} = \frac{1}{4\pi^2} \int_{\text{FS}} \frac{dA_{\mathbf{k}}}{|\nabla_{\mathbf{k}} z_{2\mathbf{k}}|}, \quad (20)$$

where m^* is the effective mass as extracted from specific-heat measurements (i.e., the effective mass of an isotropic Fermi liquid with the same γ) and $dA_{\mathbf{k}}$ is the Fermi-surface element. Under the condition that the Fermi surface can be parametrized in the way $k = k_F(\phi)$, this integral can be rewritten as

$$N_0 = \frac{m^*}{2\pi} = \frac{1}{4\pi^2} \int d\phi \frac{\sqrt{[k_F(\phi)]^2 + [k'_F(\phi)]^2}}{|\nabla_{\mathbf{k}} z_{2\mathbf{k}}|_{k=k_F(\phi)}}. \quad (21)$$

Sample results for the quasiparticle velocity, $|\nabla_{\mathbf{k}} z_{2\mathbf{k}}|_{\text{FS}}$, as a function of the Fermi-surface angle (i.e., the direction) are shown in Fig. 4 for the various hybridization cases introduced in Eq. (15). The microscopic parameters are chosen such that all four cases lead to the same value of the density of states N_0 and thus the same specific-heat coefficient. The corresponding total effective mass is around 125 times the bare c -electron mass. For $d_{x^2-y^2}$ -wave hybridization, the velocity and, therefore, also the inverse effective mass has a maximum at the nodal line ($\phi = \pi/4$)—here $m^*(\mathbf{k})$ corresponds to approximately the bare c -electron mass. Away from the nodal line, the velocity rapidly decreases. In contrast, for both s -wave-like hybridizations, the velocity is approximately constant (and small) along the Fermi surface.

The electronic quasiparticle weight $Z(\mathbf{k})$ can be easily extracted as well. Z measures the overlap between the physical c electron and the low-energy quasiparticle at the Fermi surface. In the mean-field approach of two hybridized bands, Z is given by¹⁵

$$Z(\mathbf{k}) = \frac{(z_{1\mathbf{k}} - \bar{\epsilon}_{\mathbf{k}})^2}{(z_{1\mathbf{k}} - \bar{\epsilon}_{\mathbf{k}})^2 + b^2 \beta_{\mathbf{k}}^2}. \quad (22)$$

Results for Z are displayed in Fig. 5. It is unity along the nodal lines of the hybridization but becomes very small away from it—the latter is the typical heavy-fermion situation. For the s -wave-like hybridizations, Z turns out to be independent of the momentum direction; in the s -wave case, this follows from $V_{\mathbf{k}} = \text{const}$, whereas in the extended s -wave case, this follows from the coincidence of the momentum dependence of the hybridization $V_{\mathbf{k}}$ and the c -electron dispersion $\epsilon_{\mathbf{k}}$.

At this point, let us comment on a few important issues. First, even in the presence of hybridization nodes, all local moments of the Anderson or Kondo lattice are *fully screened* in the low-temperature limit. This is obvious from the slave-boson solution which clearly describes a Fermi liquid, but also beyond slave bosons we see no reason for a (partial) breakdown of Kondo screening. For instance, in DMFT, complete screening will occur once the effective bath density of states at the Fermi level is finite (which is the case here). Physically, the local moments are entities in real space, whereas the hybridization nodes are defined in momentum space. Second, as the nodes cover only a set of momenta of zero measure, hybridization nodes do not easily lead to the so-called two-fluid behavior (i.e., a heavy Fermi liquid coexisting with local moments), which has been advocated on phenomenological grounds.²⁵ We note that these statements also hold if both quasiparticle bands (c -like and f -like) cross the Fermi level. Although one may speculate about the existence of gapless spinons at the f Fermi points where the hybridization vanishes,¹⁵ these would again cover only a set of momenta of zero measure.

C. Influence of a magnetic field

Let us briefly discuss the effects of a weak external field applied to the heavy Fermi liquid. In general, a Zeeman field

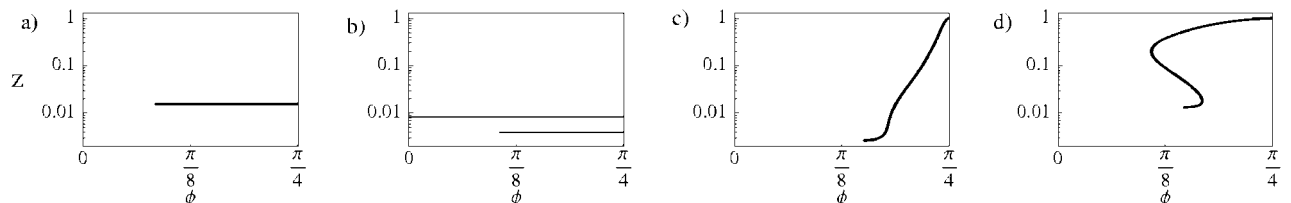


FIG. 5. As in Fig. 4, but now showing the quasiparticle weight Z in a logarithmic plot vs angle ϕ .

will cause a spin splitting of the Fermi surface, with spin- and field-dependent effective masses [or densities of states $N_\sigma(B)$].²⁶ The qualitative field dependence, $N_\sigma(B) = N_0(1 + \sigma B/B_0)$ with B_0 proportional to the Kondo temperature, is not changed by a momentum dependence of $V_{\mathbf{k}}$. [The field dependence of the mean-field parameters leads to a subleading correction $\propto B^2$ to $N_\sigma(B)$.²⁶] The anisotropy of $V_{\mathbf{k}}$, of course, causes an anisotropy of the k -space distance between the spin-split Fermi sheets, as the Fermi velocity is highly anisotropic.

For magneto-oscillation measurements, the cyclotron mass is an important quantity, given by $2\pi m_c = \partial A(E)/\partial E$, where $A(E)$ is the area enclosed by the quasiparticle isoenergy curve in a momentum-space plane perpendicular to the applied orbital field. Thus, in dimensions $d > 2$, the cyclotron mass m_c depends on the field direction. However, in two dimensions, this dependence is absent, and m_c is identical to the (averaged) quasiparticle mass m^* extracted from the density of states or specific heat, independent of momentum-space anisotropies.

D. Optical conductivity

The optical response of heavy-fermion metals has been studied extensively.⁸ Experiments probing the optical conductivity $\sigma(\omega)$ usually show a Drude peak well separated from midinfrared excitations. These features have been interpreted in the two-band picture advocated above. While intraband particle-hole excitations produce conventional metallic Drude-like response, interband excitations lead to finite weight at elevated energies. In a picture of free fermions, the threshold energy of these optical interband excitations measures the minimum gap between occupied and unoccupied states in the lower and upper bands, respectively. For momentum-independent hybridization between c and f bands, this optical gap Δ_{opt} is simply given by twice the value of the renormalized hybridization. As explained above, the hybridization is expected to scale as the square root of the coherence temperature; hence, $\Delta_{\text{opt}} \sim \sqrt{T_{\text{coh}}}D$ (where D is the conduction-electron bandwidth). Clearly, the simple two-band picture falls short of capturing inelastic processes at nonzero energies, which will inevitably smear out the gap even at $T=0$. Nevertheless, a pseudogaplike feature has been shown to survive in $\sigma(\omega)$ when fully accounting for dynamic local correlation effects in the framework of DMFT for the standard Anderson lattice model at large U .^{21,27} In the results of these calculations, the magnitude of the pseudogap has the same scaling as above, $\Delta_{\text{opt}} \sim \sqrt{T_{\text{coh}}}$. Remarkably, this relation between optical gap and coherence temperature has been found to be nicely obeyed by a number of heavy-fermion metals.⁸⁻¹² However, optical-conductivity studies in CeMIn_5 ($M=\text{Ir, Rh, or Co}$) show little signatures of a well-defined hybridization gap.⁷ As we show below, such a behavior is, in principle, consistent with a strongly momentum-dependent hybridization in the underlying Anderson lattice model.

The finite-frequency part of the optical conductivity $\sigma(\omega)$ can be expressed through the retarded current-current correlation function as

$$\sigma(\omega) = \frac{i}{\omega} \Pi(\omega + i\eta), \quad (23)$$

with

$$\Pi(i\omega) = - \int_0^\beta d\tau e^{i\omega\tau} \langle T_\tau \mathbf{j}^\dagger(\tau) \mathbf{j}(0) \rangle. \quad (24)$$

The current operator \mathbf{j} has to be calculated as the time derivative of the polarization operator \mathbf{P} ,

$$\mathbf{j} = i[\mathcal{H}, \mathbf{P}], \quad (25)$$

where the definition of \mathbf{P} includes all charged particles a_i (with charge q_i),

$$\mathbf{P} = \sum_{i\sigma} q_i \mathbf{R}_i a_i^\dagger a_i. \quad (26)$$

As usual, approximations to the propagators and to the current vertex in calculating $\Pi(\omega)$ have to be mutually consistent in order to respect charge conservation (expressed by the corresponding Ward identity).

At this point, the electrodynamics of the heavy Fermi liquid requires a thorough discussion. Physically, the f electrons contribute to the Fermi surface and carry charge. While this is plausible in the Anderson model picture, where the charge is naturally carried by the \bar{f} auxiliary particles, the Kondo case is more subtle. The \bar{f} particles of the mean-field theory are neutral spinons, which will carry a physical electric charge only upon inclusion of gauge fluctuations, see Sec. V. Hence, we shall take the Anderson model viewpoint here. In the spirit of the mean-field theory, we demand the current correlator to be calculated as the bare bubble. An expression for the current vertex, which is consistent with the mean-field propagators, is obtained from

$$\mathbf{j}_{\text{MF}} = i[\mathcal{H}_{\text{ALM, MF}}, \mathbf{P}_{\text{MF}}], \quad (27)$$

where charge-carrying particles c_i and \bar{f}_i are contained in \mathbf{P}_{MF} ,

$$\mathbf{P}_{\text{MF}} = \sum_{i\sigma} \mathbf{R}_i (c_{i\sigma}^\dagger c_{i\sigma} + \bar{f}_{i\sigma}^\dagger \bar{f}_{i\sigma}). \quad (28)$$

Evaluating Eq. (27) leads to

$$\mathbf{j}_{\text{MF}} = \sum_{\mathbf{k}\sigma} [(\nabla_{\mathbf{k}} \epsilon_{\mathbf{k}}) c_{\mathbf{k}\sigma}^\dagger c_{\mathbf{k}\sigma} + r(\nabla_{\mathbf{k}} V_{\mathbf{k}})(c_{\mathbf{k}\sigma}^\dagger \bar{f}_{\mathbf{k}\sigma} + \text{H.c.})]. \quad (29)$$

Let us pause to emphasize that a current operator derived from \mathcal{H}_{ALM} before the mean-field approximation would have an f -electron contribution different from that in \mathbf{j}_{MF} , but such a current vertex would be *inconsistent* when used together with the bubble of mean-field propagators, i.e., vertex corrections would become important. We point out that \mathbf{j}_{MF} has several shortcomings because \mathbf{P}_{MF} treats \bar{f} as real electrons; nevertheless, expression (29) is the *only* current operator suitable within the mean-field treatment of the Anderson model. We also note that the second term in \mathbf{j}_{MF} vanishes in the conventional case of a constant hybridization $V_{\mathbf{k}}$, and

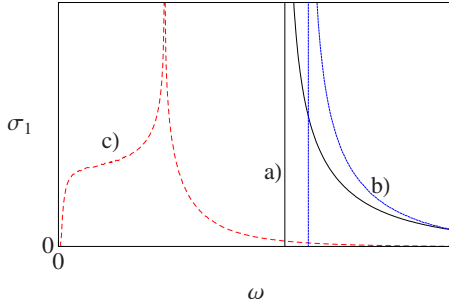


FIG. 6. (Color online) Real part of the optical conductivity $\sigma_1(\omega)$ for (a) s -wave (solid), (b) extended s -wave (dotted), and (c) $d_{x^2-y^2}$ -wave hybridization (dashed). The parameters are as in Figs. 2(a)–2(c), for a discussion, see text.

ambiguities regarding the treatment of the f electrons do not arise.^{21,28}

Using the current operator \mathbf{j}_{MF} [Eq. (29)], the expression for the real part of the optical conductivity σ_1 (still assuming $n_c < 1$) reads

$$\sigma_1(\omega) = \frac{\pi}{\omega} \sum_{\mathbf{k}} \frac{n_F(z_{2\mathbf{k}})}{(z_{1\mathbf{k}} - z_{2\mathbf{k}})^2} A_{\mathbf{k}} \delta(z_{1\mathbf{k}} - z_{2\mathbf{k}} - \omega), \quad (30)$$

using the abbreviations $\tilde{\epsilon}_f = \epsilon_f - \lambda$ and

$$A_{\mathbf{k}} = (\nabla_{\mathbf{k}} \epsilon_{\mathbf{k}})^2 (z_{2\mathbf{k}} - \tilde{\epsilon}_f)(z_{1\mathbf{k}} - \tilde{\epsilon}_f) + r^2 (\nabla_{\mathbf{k}} V_{\mathbf{k}})^2 [(z_{1\mathbf{k}} - z_{2\mathbf{k}}) + 4r^2 V_{\mathbf{k}}^2] + 2r^2 V_{\mathbf{k}} \nabla_{\mathbf{k}} \epsilon_{\mathbf{k}} \nabla_{\mathbf{k}} V_{\mathbf{k}} (z_{2\mathbf{k}} + z_{1\mathbf{k}} - 2\tilde{\epsilon}_f). \quad (31)$$

The result for $\sigma(\omega > 0)$ from a numerical evaluation of Eq. (30) is depicted in Fig. 6, for the three hybridization symmetries of Eq. (15) and parameters as in Figs. 2(a)–2(c). In all situations, a finite gap Δ_{opt} is visible in $\sigma(\omega)$, which corresponds to the minimal direct gap between the two bands $z_{1\mathbf{k}}$ and $z_{2\mathbf{k}}$. In the cases of the s -wave and the extended s -wave hybridization, Δ_{opt} is given by $2b$ and $|\lambda_0 - \mu|b/\sqrt{b^2 + t^2}$, respectively; both expressions translate into $\Delta_{\text{opt}} \sim \sqrt{T_{\text{coh}} D}$ (up to prefactors), as known before. For $d_{x^2-y^2}$ -wave hybridization, the two bands cross along the nodal lines, but this crossing is at a finite energy away from the Fermi level. Hence, the direct gap is finite and given by the renormalized f level position, $|\lambda_0|$ —this translates into $\Delta_{\text{opt}} \propto T_{\text{coh}}$. Above this threshold energy, the optical conductivity follows $\sqrt{\omega - \Delta_{\text{opt}}}$, see Appendix C.

As discussed above, a hard gap in $\sigma(\omega)$ will not survive beyond mean field, but we expect the qualitative result to remain valid. We therefore conclude that a hybridization $V_{\mathbf{k}}$ with momentum-space nodes leads to transfer of optical spectral weight from the energy scale $\sqrt{T_{\text{coh}} D}$ to the scale T_{coh} (when compared to the case of constant hybridization). For actual experiments, this likely implies that no hybridization gap will be visible in the optical conductivity, due to the finite width of the Drude peak. Such a scenario is qualitatively consistent with the optical-conductivity data obtained on CeMIn_5 .⁷

E. Thermal transport

Low-temperature dc transport quantities are, in principle, candidates to probe strong anisotropies in momentum space. As an example, let us consider the thermal conductivity (which sometimes shows less sample dependence than the electrical conductivity). The energy current operator in the mean-field approximation reads¹⁴

$$\mathbf{j}_T = \sum_{\mathbf{k}\sigma} [z_{1\mathbf{k}} (\nabla_{\mathbf{k}} z_{1\mathbf{k}}) \gamma_{1\mathbf{k}}^\dagger \gamma_{1\mathbf{k}} + (1 \leftrightarrow 2)], \quad (32)$$

where $\gamma_{1,2}^\dagger$ are the operators creating a quasiparticle in the $z_{1,2}$ band. From the Kubo formula, one derives the low-temperature thermal conductivity in relaxation-time approximation,

$$\kappa_{ij} = \frac{1}{T} \sum_{\mathbf{k}\sigma} z_{2\mathbf{k}}^2 (\nabla_{\mathbf{k}} z_{2\mathbf{k}})_i (\nabla_{\mathbf{k}} z_{2\mathbf{k}})_j [-n'_F(z_{2\mathbf{k}})] \frac{1}{\Gamma(z_{2\mathbf{k}})}, \quad (33)$$

where Γ denotes the impurity-induced quasiparticle scattering rate, and we have again assumed that only the band $z_{2\mathbf{k}}$ crosses the Fermi level.

As already discussed by Moreno and Coleman¹⁴ in the context of gap-anisotropic Kondo insulators, the thermal conductivity will be strongly anisotropic for three-dimensional systems where the hybridization has, e.g., line nodes. In contrast, in the 2D case of a $d_{x^2-y^2}$ hybridization, the conductivity tensor does not have enough degrees of freedom to reflect the anisotropy, as the two principal axes are equivalent here. (The sign of $\beta_{\mathbf{k}}$ does not enter.) The same applies to hybridization functions $V_{\mathbf{k}}$ with higher angular momenta l . Hence, for 2D anisotropic systems, higher-order correlation functions need to be considered, as e.g., probed by angle-dependent magnetoresistance; this is beyond the scope of this paper. [An exception is a p -wave hybridization (i.e., $l=1$), which explicitly breaks the C_4 rotation symmetry down to C_2 , leading to an in-plane transport anisotropy. Note that such a hybridization will be accompanied by a corresponding lattice distortion, which will be reflected in the entire band structure.]

Finally, we note that, independent of possible transport anisotropies, the Wiedemann–Franz law will always be obeyed (assuming elastic scattering only): The Lorenz number L , formed from the thermal conductivity κ_{ii} and the electrical conductivity σ_{ii} via $L = \kappa/(\sigma T)$, will approach the constant $L_0 = (\pi^2/3)(k_B/e)^2$ in the low-temperature limit. This is consistent with the fact that we are describing a Fermi liquid. As a corollary, the recently observed violation of the Wiedemann–Franz law in CeCoIn_5 at its field-induced critical point²⁹ is likely related to inelastic scattering processes.

V. BEYOND MEAN-FIELD THEORY

So far, we have discussed the low-temperature properties of “unconventional” heavy Fermi liquids using slave-boson mean-field theory. In principle, corrections to mean-field theory can be systematically taken into account, by considering fluctuations around the saddle point. For the Kondo model, the correct implementation of the Hilbert space constraint, together with phase fluctuations of the boson field,

leads to a theory where \tilde{f} and b particles are minimally coupled to a compact U(1) gauge field. The Fermi-liquid phase corresponds to the Higgs/confining phase of the gauge theory; it is stable with respect to fluctuation effects, their main effect being to endow the \tilde{f} particle with a physical electric charge.^{30,31}

To treat the full crossover from energies or temperatures above T_K to those below T_{coh} , different methods need to be employed. Local correlations can be efficiently captured by DMFT.²⁰ If DMFT is formulated for the Anderson lattice model [Eq. (1)], correlation effects arise from the *local* Hubbard interaction U and, consequently, DMFT can be used to treat an Anderson model with nonlocal hybridization $V_{\mathbf{k}}$ as well. The DMFT self-consistency equation then reads

$$\begin{aligned} G_{\text{ALM,loc}}(z) &= \sum_{\mathbf{k}} \frac{1}{z - \epsilon_f - \Sigma_f(z) - \frac{V_{\mathbf{k}}^2}{z - \bar{\epsilon}_{\mathbf{k}}}} \\ &= \frac{1}{z - \epsilon_f - \tilde{\Delta}(z) - \Sigma_f(z)} = G_{\text{SIAM}}(z). \end{aligned} \quad (34)$$

Here, Σ_f is the so-called interaction self-energy arising from U , and $\tilde{\Delta}$ denotes the effective hybridization function defined by the second line of Eq. (34). While we shall not numerically solve the DMFT problem [Eq. (34)] here, we can briefly discuss a few properties. Most importantly, the momentum dependence of the arising effective hybridization is dictated by the bare $V_{\mathbf{k}}$. This implies that all qualitative statements in Sec. IV remain valid, in particular, all local moments will be fully screened at low T . [Technically, the DMFT reduces the lattice model [Eq. (1)] to an effective single-impurity model, with a bath having a finite density of states at the Fermi level—this implies a fully developed Kondo effect as $T \rightarrow 0$.]

Cluster extensions of DMFT allow us to handle momentum-dependent self-energies. Then, in principle, the momentum dependence of the effective hybridization will differ from that of the bare $V_{\mathbf{k}}$. However, we do not expect qualitative changes of the low-temperature physics described above.

Let us note one caveat: While calculating thermodynamics and single-particle properties within DMFT for the Anderson model [Eq. (1)] is straightforward, electric transport is not. The reason is that the current operator inevitably involves contributions from the nonlocal hybridization, see discussion in Sec. IV D. As a result, vertex corrections do not vanish in the DMFT limit, in contrast to standard DMFT applications.²⁰

VI. TEMPERATURE-DEPENDENT RESISTIVITY

In this section, we touch upon electronic properties at elevated temperatures. In particular, we want to focus on the electrical resistivity $\rho(T)$ of heavy fermions with unconventional hybridization for $T > T_K$.

In the conventional heavy-fermion picture, the electrical resistivity $\rho(T)$ at high temperatures, $T \gg T_K$, is small (ignor-

ing phonons here), and $\rho(T)$ rises upon lowering the temperature due to increasing magnetic scattering. At a scale which is often identified with the lattice coherence temperature T_{coh} , $\rho(T)$ reaches a maximum and then drops upon further cooling, behaving as $\rho(T) = \rho_0 + AT^2$ at low T . At elevated temperatures, $T > T_K$, the scattering can be accessed using perturbation theory in the Kondo coupling, i.e., the physical picture is that of c electrons (with a small Fermi surface) scattering inelastically off the f moments.

Bare perturbation theory gives a single-particle scattering rate

$$\tau_{\mathbf{k}}^{-1} \propto J_0^2 \beta_{\mathbf{k}}^2 \left(1 + \frac{J_0}{D} \ln \frac{D}{T} \right). \quad (35)$$

A few remarks are in order. (i) In the paramagnetic phase of a Kondo lattice, all contributions to the conduction-electron self-energy up to order J_0^3 arise from single-impurity scattering. (ii) The prefactor $\beta_{\mathbf{k}}^2$ comes from the two external lines of the self-energy diagrams, whereas the internal momentum summations average out all other form factors—this is also true for higher-order diagrams. Assuming that scattering arises from the local moments only, the simplest approximation for the conductivity $\sigma \propto 1/\rho$ yields

$$\sigma_{ij}(T) \propto \int_{\text{FS}} \frac{d^{d-1}k}{(2\pi)^d} v_i(\mathbf{k}) v_j(\mathbf{k}) \tau_{\mathbf{k}}, \quad (36)$$

where $v_i(\mathbf{k}) = d\epsilon_{\mathbf{k}}/dk_i$ is the quasiparticle velocity. The result [Eqs. (35) and (36)] is interesting, as it shows that for form factors $\beta_{\mathbf{k}}$ with nodes, the Kondo scattering is *insufficient* to render the conductivity finite because $\tau_{\mathbf{k}}$ diverges at least like $(k - k_n)^{-2}$ near the node at k_n . The physical origin is that conduction electrons with momenta at the hybridization nodes are not scattered at all, and this short circuits all other processes, leading to *infinite* conductivity. To obtain a finite conductivity, additional scattering needs to be considered, namely, electron-electron scattering among the conduction electrons, electron-lattice scattering, or scattering off static impurities. The resulting interplay of scattering mechanisms can be complex and can even modify the basic temperature dependence of $\rho(T)$, but we shall not analyze it here in detail.

The physical conclusion is that the electrical current, at least in the temperature regime $T > T_K$, is primarily carried by conduction electrons with weak hybridization to the f moments; hence, “nodal” quasiparticles dominate the electric transport. Recall that, in contrast, the low-temperature thermodynamics is dominated by “antinodal” quasiparticles.

VII. COMPETITION BETWEEN KONDO SCREENING AND ORDERING

As already discussed by Doniach,³² the phase diagram of heavy-fermion metals is determined by the competition between Kondo effect and intermoment exchange [either of direct or Ruderman–Kittel–Kasuya–Yoshida (RKKY) type]. Intermoment exchange can drive magnetic ordering but may also lead to nontrivial metallic spin-liquid states and to magnetically mediated superconductivity. The competition with Kondo screening may be simply understood by stating that

the local f moments can either form Kondo singlets with the conduction electrons or they can order in a symmetry-breaking fashion or else pair into intermoment singlets.

Thinking about these competing tendencies in momentum space, it is conceivable that, in a situation with momentum-space differentiation of electronic band properties, certain ordering phenomena are favored or disfavored by a given form of the hybridization. This idea will be illustrated in this section, using magnetically mediated superconductivity as an example, where one can expect an intricate interplay between hybridization and pairing symmetries. Concrete calculations will be performed for a Kondo–Heisenberg model in a mean-field approach. As in Ref. 33, a magnetic interaction between the f moments can be decoupled in the particle-particle channel, leading to pairing of spinons, which, if coexisting with Kondo screening, leads to BCS-type superconductivity.

A. Kondo–Heisenberg model

The Anderson and Kondo lattice models [Eqs. (1) and (2)] contain the competition of Kondo and RKKY interactions. However, in the slave-boson approach, the effect of the RKKY interaction is lost. For mean-field calculations, it is thus convenient to introduce an explicit intermoment exchange interaction of Heisenberg type,

$$\mathcal{H}_H = \sum_{ij} \frac{J_{H,ij}}{2} \mathbf{S}_i \cdot \mathbf{S}_j. \quad (37)$$

The physics of the model $\mathcal{H}_{\text{KLM}} + \mathcal{H}_H$, commonly referred to as the Kondo–Heisenberg model, has been extensively discussed in the literature. We shall give a comprehensive discussion of all phases and phase diagrams but instead concentrate on the possible emergence of superconductivity due to f -electron pairing. A general framework has been laid out in Refs. 33 and 34, which considered a scenario where dominant RKKY interaction does not lead to antiferromagnetism but instead to a metallic spin-liquid state. This state, arising, e.g., from geometric frustration of the intermoment exchange, has been dubbed “fractionalized Fermi liquid” (FL*), as it features light conduction electrons, forming a Fermi liquid, which coexist with a fractionalized spin liquid formed out of the f electrons. Then, in the generalized Doniach phase diagram, the heavy Fermi liquid (FL) is separated from FL* by a quantum critical point where Kondo screening breaks down, but no local symmetries are broken.^{33,34} (This quantum critical point has been discussed in relation to unconventional quantum criticality in materials such as CeCu_{6-x}Au_x and YbRh₂Si₂.)

A specific realization of FL* is a state with paired spinons and an emergent Z_2 gauge structure. As detailed in Ref. 33, one can expect magnetically mediated superconductivity close to the quantum critical point between FL and a Z_2 FL*. All resulting low-temperature phases can be conveniently described in a mean-field approach, where the standard slave-boson description of the Kondo effect is combined with a Sp(2N) mean-field treatment of the Heisenberg exchange.³⁵ Below, we shall extend this mean-field theory to the case of momentum-dependent hybridization.

B. Mean-field theory and magnetically mediated superconductivity

A mean-field theory for the Kondo–Heisenberg model, $\mathcal{H}_{\text{KLM}} + \mathcal{H}_H$, involves a decoupling of the Kondo interaction as in Sec. III and of the intermoment Heisenberg exchange \mathcal{H}_H . Using the pseudofermion representation of the local moments as above, nonlocal spinon pairing is described by a mean field of the form $\Delta_{ij} = -\langle \tilde{f}_{i\uparrow} \tilde{f}_{j\downarrow} - \tilde{f}_{i\downarrow} \tilde{f}_{j\uparrow} \rangle$. Then, the Heisenberg interaction can be written at the mean-field level as³⁶

$$\mathcal{H}_{H,\text{MF}} = - \sum_{ij} \frac{J_{H,ij}}{4} [(2\Delta_{ij} \tilde{f}_{i\uparrow}^\dagger \tilde{f}_{j\downarrow}^\dagger + \text{H.c.}) - |\Delta_{ij}|^2]. \quad (38)$$

For time-reversal invariant states, the bond field $\Delta_{ij} = \Delta_{ji}$ can be chosen to be real. Importantly, the mean-field Hamiltonian [Eq. (38)] is the exact solution of the Heisenberg model in the symplectic Sp(2N) large- N limit, with a fully antisymmetric representation of the local moments.³⁵ (This large- N limit uniquely selects the particle-particle decoupling of the Heisenberg interaction.³⁶) Physicwise, nonzero Δ_{ij} creates a paramagnetic phase out of the f moments; in particular, uniform Δ_{ij} describes a gapped Z_2 spin liquid but also states with broken translational symmetry can occur which can be classified as valence-bond solids.³⁸ A consistent Sp(2N) mean-field treatment of the full model $\mathcal{H}_{\text{KLM}} + \mathcal{H}_H$ is obtained by also decoupling the Kondo interaction in the particle-particle channel. However, one can show that for the Kondo part, both particle-hole and particle-particle decoupling schemes are equivalent regarding physical observables, provided that $n_f = 1$ and time-reversal symmetry is present.

The full mean-field theory is now given by $\mathcal{H}_{\text{KLM, MF}} + \mathcal{H}_{H,\text{MF}}$, with the two “order parameters” b and Δ . Restricting ourselves to states without translational symmetry breaking, the following mean-field phases occur. At high temperatures, a trivial decoupled phase with $b = \Delta = 0$ is realized. If the Heisenberg exchange J_H dominates over the Kondo coupling J_0 , then Δ will be finite, and b zero at low T , resulting in decoupled c - and f -electron subsystems. This is the FL* phase described above. On the other hand, nonzero b and vanishing Δ describe a conventional heavy FL (which was the subject of Sec. III). Finally, if both Δ and b are nonzero, Kondo screening coexists with spinon pairing, which leads to a true superconducting (SC) state, with pairing mediated by the magnetic coupling among the f moments. At sufficiently low T , the FL phase is always unstable toward superconductivity in the presence of a nonzero J_H . (Note that the FL* phase is not a superconductor, as the \tilde{f} particles do not carry a physical charge in the absence of Kondo screening.) Fluctuation corrections to mean-field theory will smear out the finite-temperature transitions of the FL and FL* phases (the latter only in $d=2$ dimensions), whereas the superconducting transition remains a true phase transition.³³

At this point, a more detailed discussion of the spatial structure of the Heisenberg interaction, described by $J_{H,ij}$, and of the resulting pairing is needed. For nearest-neighbor exchange on the square lattice of f moments, each unit cell contains two bond variables, Δ_{ij} . A numerical solution shows

that two types of saddle points exist (provided that translational and time-reversal invariances are imposed³⁸), namely, a uniform (or “extended s -wave”) solution with $\Delta_{ij}=\Delta$ on all links and a “ $d_{x^2-y^2}$ -wave” solution with $\Delta_{ij}=\pm\Delta$ on horizontal and vertical links, respectively. We will also consider the case where $J_{H,ij}$ only act on next-neighbor diagonal bonds, which together with an alternating structure of the Δ_{ij} leads to a “ d_{xy} -wave” mean-field solution of the Heisenberg part. All cases can be written in momentum space as

$$\mathcal{H}_{H,MF} = \sum_{\mathbf{k}} \tilde{W}_{\mathbf{k}} (\tilde{f}_{\mathbf{k}\uparrow}^\dagger \tilde{f}_{-\mathbf{k}\downarrow}^\dagger + \text{H.c.}) + J_H \mathcal{N} \Delta^2, \quad (39)$$

with the abbreviation $\tilde{W}_{\mathbf{k}} = -J_H \Delta \alpha_{\mathbf{k}}$, and $\alpha_{\mathbf{k}}$ contains the “form factor” of the spinon pairing,

$$\alpha_{\mathbf{k}} = \begin{cases} \cos k_x + \cos k_y & \text{extended } s \text{ wave} \\ \cos k_x - \cos k_y & d_{x^2-y^2} \text{ wave} \\ 2 \sin k_x \sin k_y & d_{xy} \text{ wave.} \end{cases} \quad (40)$$

The self-consistency equation which supplements the Hamiltonian $\mathcal{H}_{KLM,MF} + \mathcal{H}_{H,MF}$ is given by Eqs. (12a)–(12c) and

$$\sum_{\mathbf{k}} \alpha_{\mathbf{k}} \langle \tilde{f}_{\mathbf{k}\uparrow}^\dagger \tilde{f}_{-\mathbf{k}\downarrow}^\dagger + \text{H.c.} \rangle = 2\mathcal{N}\Delta. \quad (41)$$

All expectation values can again be expressed in terms of Green functions, see Appendix A 2. Diagonalizing the mean-field Hamiltonian, we obtain the quasiparticle energies

$$\begin{aligned} \bar{z}_{1,2,3,4\mathbf{k}} = & \pm \frac{1}{\sqrt{2}} \{ \lambda_0^2 + \bar{\epsilon}_{\mathbf{k}}^2 + 2b^2 \beta_{\mathbf{k}}^2 + \tilde{W}_{\mathbf{k}}^2 \pm [-4(\lambda_0 \bar{\epsilon}_{\mathbf{k}} + b^2 \beta_{\mathbf{k}}^2)^2 \\ & - 4\bar{\epsilon}_{\mathbf{k}}^2 \tilde{W}_{\mathbf{k}}^2 + (\lambda_0^2 + \bar{\epsilon}_{\mathbf{k}}^2 + 2b^2 \beta_{\mathbf{k}}^2 + \tilde{W}_{\mathbf{k}}^2)^2]^{1/2} \}^{1/2}. \end{aligned} \quad (42)$$

Let us point out an interesting feature of the SC state. Due to the momentum-dependent hybridization, the internal structure of the Cooper pairs is highly nontrivial. In particular, the anomalous expectation value of the physical electrons is given by $\langle c_{\mathbf{k}\uparrow}^\dagger c_{-\mathbf{k}\downarrow}^\dagger \rangle \propto \Delta \beta_{\mathbf{k}}^2 \alpha_{\mathbf{k}} M_{\mathbf{k}}$, where $M_{\mathbf{k}}$ is a smooth function respecting the lattice symmetries (see Appendix A 2). This transforms under the same representation of the space group as the $\langle \tilde{f}_{\mathbf{k}\uparrow}^\dagger \tilde{f}_{-\mathbf{k}\downarrow}^\dagger \rangle \propto \Delta \alpha_{\mathbf{k}}$ of the spinons but has additional zeros from $\beta_{\mathbf{k}}^2$. (A somewhat similar situation appears in the composite pairing picture of Ref. 37, however, there arising from two-channel Kondo physics.) The additional zeros will have a strong influence on thermodynamics, e.g., the power law in the low-temperature specific heat will be modified.

C. Qualitative discussion: $T_c \ll T_K$ versus $T_c \sim T_K$

Pairing in a Kondo lattice system can occur in qualitatively different regimes, depending on the relation between the superconducting T_c and the characteristic Kondo scale. If $T_c \ll T_K$, then the proper picture is that of BCS-like pairing out of a well-formed heavy Fermi liquid. In contrast, $T_c \sim T_K$ implies a strong competition of Kondo screening and Cooper pairing, and superconductivity emerges out of an incoherent non-Fermi-liquid regime. (The formal situation T_c

$\gg T_K$ leads to the nonsuperconducting FL* phase.)

Let us quickly discuss the two regimes in the framework of the mean-field theory, keeping in mind that inelastic processes at energies of order T_K will not be captured. The mean-field equation [Eq. (41)] reduces to an equation for T_c if we set Δ to zero,

$$\frac{2}{J_H} = \frac{1}{\mathcal{N}} \sum_{\mathbf{k}} \alpha_{\mathbf{k}}^2 \left[\frac{z_{1\mathbf{k}}^2 - \bar{\epsilon}_{\mathbf{k}}^2}{z_{1\mathbf{k}}^2 - z_{2\mathbf{k}}^2} \frac{1}{z_{1\mathbf{k}}} \tanh \frac{z_{1\mathbf{k}}}{2T_c} + (1 \leftrightarrow 2) \right]. \quad (43)$$

The factor $\alpha_{\mathbf{k}}^2$ originates from the fact that the momentum dependencies of both the gap and the pairing interaction $\tilde{W}_{\mathbf{k}}$ are equal by construction.

In the regime $T_c \ll T_K$, only the quasiparticle band crossing the Fermi level (which we again assume to be $z_{2\mathbf{k}}$) contributes to pairing. We replace the \mathbf{k} summation by an integral over isoenergetic lines $\int d\omega \int_{\omega=z_{2\mathbf{k}}} dA_{\mathbf{k}} / |\nabla z_{2\mathbf{k}}|$. In analogy to the standard BCS case we approximate $\tanh(\omega/2T_c) = 1$ for $\omega \geq 2T_c$ and 0 elsewhere. The factor of $\alpha_{\mathbf{k}}^2$ will be taken at its value at the Fermi surface. Furthermore, we will set $\kappa \equiv (\bar{\epsilon}_{\mathbf{k}}^2 - z_{2\mathbf{k}}^2) / (z_{1\mathbf{k}}^2 - z_{2\mathbf{k}}^2) \approx \text{const}$, assuming that it is weakly varying along the Fermi surface. Neglecting the dependencies of the velocity and $\alpha_{\mathbf{k}}$ perpendicular to the Fermi surface, we obtain

$$\frac{2}{J_H} = \int_{2T_c}^{\Lambda} \frac{d\omega}{\omega} \int_{\text{FS}} \frac{dA_{\mathbf{k}}}{2\pi} \frac{\kappa \alpha_{\mathbf{k}}^2}{|\nabla_{\mathbf{k}} z_{2\mathbf{k}}|}, \quad (44)$$

with Λ of order the bandwidth. This gives a rough T_c estimate of

$$T_c = \frac{\Lambda}{2} \exp \left[- \frac{4\pi}{J_H \kappa \int dA_{\mathbf{k}} (\alpha_{\mathbf{k}}^2 / |\nabla_{\mathbf{k}} z_{2\mathbf{k}}|)} \right]. \quad (45)$$

This equation shows the direct interplay of the form factors: T_c is enhanced if the pairing is strong (large $\alpha_{\mathbf{k}}$) in regions where quasiparticles are heavy and hence have large f character. In other words, antinodal regions along the Fermi surface with large hybridization are more susceptible to pairing.

In contrast, in the regime of $T_c \sim T_K$, both bands contribute to pairing, and one can expect large contributions to the integral in Eq. (43) from the essentially flat parts of both bands $z_{1,2\mathbf{k}}$, which are present, in particular, close to the nodal lines of the hybridization $V_{\mathbf{k}}$. This simple argument illustrates the competition between Kondo effect and pairing in the regime $T_c \sim T_K$. Nodal momentum-space regions with less hybridization are more susceptible to pairing—this is opposite to the statement made above for $T_c \ll T_K$. One should, however, keep in mind that the mean-field theory has limited relevance for the true physics at energies or temperatures of order T_K , the key point being that electrons in the antinodal regions are rather incoherent. The emerging problem of the pairing of incoherent fermions is of fundamental relevance and heavily debated, for instance, in the field of high-temperature superconductors but rather little solid

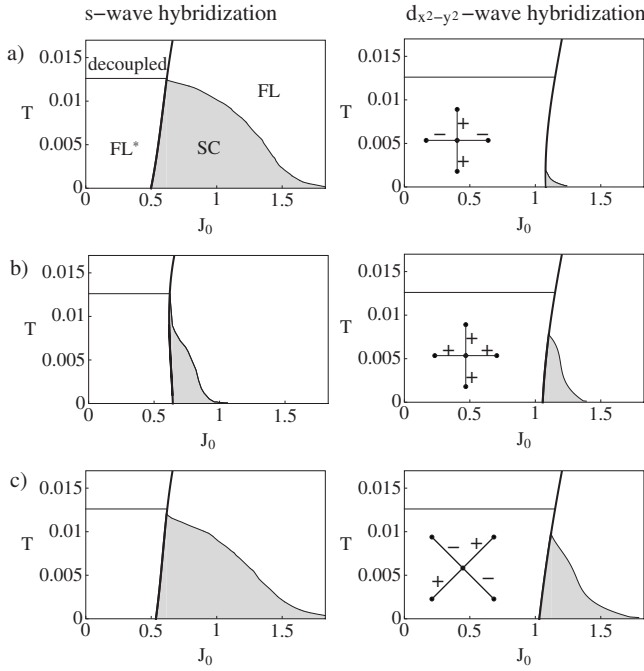


FIG. 7. Phase diagrams in dependence of temperature T and Kondo coupling J_0 at $n_c=0.3$ for an extended s - and a $d_{x^2-y^2}$ -wave hybridization, combined with different types of a superconducting symmetry: (a) $d_{x^2-y^2}$ wave, (b) extended s wave, and (c) d_{xy} wave. The left-panel insets show the real-space structure of spinon pairing fields Δ_{ij} , leading to the certain type of pairing symmetry. Thick (thin) lines refer to first- (second-) order phase transitions; for further details, see text.

knowledge exists about this highly interesting strong-coupling phenomenon.

D. Extended phase diagrams

The discussion of the last section suggests that a certain hybridization symmetry can favor or disfavor a certain pairing symmetry. To follow up on this idea, we have determined mean-field phase diagrams from a fully self-consistent numerical solution of Eqs. (12) and (41). While our results, in principle, support the above statement, they also show that microscopic details of band structure, band filling, and pairing interaction are important in determining T_c (which may render simplistic arguments invalid).

Sample phase diagrams as a function of temperature T and Kondo coupling J_0 , keeping J_H , t , and n_c fixed, are shown in Fig. 7, for hybridizations of extended s - and $d_{x^2-y^2}$ -type and various pairing symmetries. The overall structure of the phase diagram was discussed above in Sec. VII B and is identical to that described in Ref. 33.

The different pairing symmetries in Fig. 7 have to be understood as follows. For a given Heisenberg interaction, saddle points with different spinon pairing symmetry occur, and to plot the phase diagrams, we have restricted our attention by hand to one of the saddle points. The correct superconducting phase is obtained by comparing the free energies, given by the mean-field expression

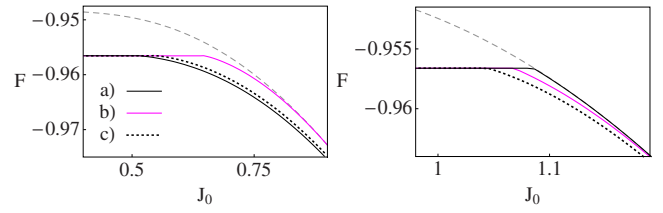


FIG. 8. (Color online) Free energy plotted against the Kondo coupling J_0 at $n_c=0.3$ and $T=10^{-5}$ for extended s -wave hybridization (left) and $d_{x^2-y^2}$ -wave hybridization (right) and different superconducting symmetries: (a) $d_{x^2-y^2}$ wave, (b) extended s wave, and (c) d_{xy} wave (compare to the corresponding phase diagrams shown in Fig. 7). The thin dashed line shows the normal-state solution with $\Delta=0$.

$$F = -\frac{1}{\beta} \sum_{\mathbf{k}, i} \ln(1 + e^{-\beta \tilde{\epsilon}_{\mathbf{k}, i}}) + \sum_{\mathbf{k}} (\epsilon_{\mathbf{k}} - \lambda_0) + \mathcal{N} \mu n_c + \mathcal{N} \lambda_0 + \mathcal{N} J_H \Delta^2 + \mathcal{N} \frac{b^2}{J_0}. \quad (46)$$

Plots of the free energies at low T are presented in Fig. 8.

The rough conclusion for the particular dispersion and band filling used here is that extended s -wave hybridization favors the $d_{x^2-y^2}$ -wave superconducting symmetry, while $d_{x^2-y^2}$ -wave hybridization favors d_{xy} -wave superconductivity. Given the structure of the Fermi surfaces in the FL phase, this is not unexpected. If both $\alpha_{\mathbf{k}}$ and $\beta_{\mathbf{k}}$ have an extended s structure, the pairing interaction is rather small near the Fermi surface [Fig. 2(b)] and, consequently, the superconductivity is weak in the left panel of Fig. 7(b), whereas both d -wave pairing states perform nicely in energy. For $\beta_{\mathbf{k}}$ of $d_{x^2-y^2}$ form, the Fermi surface [Fig. 2(c)] is mainly located close to the momentum-space diagonals, favoring d_{xy} pairing [right panel of Fig. 7(c)].

VIII. CONCLUSIONS

In this paper, we have explored the consequences of a strongly momentum-dependent hybridization between conduction and local-moment electrons in heavy-fermion metals. In the Fermi-liquid regime, the quasiparticle properties become strongly anisotropic along the Fermi surface: “nodal” quasiparticles are light c electrons, whereas “antinode” quasiparticles are heavy and have essentially f character. An interesting dichotomy arises: while the low-temperature thermodynamics is dominated by heavy antinodal quasiparticles, the electrical conductivity at elevated temperatures is carried by unhybridized nodal quasiparticles. Experimentally important is the low-temperature optical conductivity $\sigma(\omega)$. Due to the strongly momentum-dependent gap between the effective bands, the hybridization gap in $\sigma(\omega)$ is essentially smeared out.

Further, we have advocated the idea that the momentum-space structure of the hybridization is important in selecting ordering phenomena which compete with Kondo screening near quantum criticality. Here, two regimes need to be distinguished. For energies or temperatures T much smaller than

the coherence temperature T_{coh} , a weak-coupling quasiparticle picture is often appropriate, and instabilities of the heavy Fermi liquid are determined by the interaction among the (anisotropic) quasiparticles. In contrast, for $T \sim T_{\text{coh}}$, fascinating strong-coupling phenomena can be expected, for example, unconventional superconductivity emerging from a non-Fermi liquid regime. This physics will be dominated by inelastic processes, which again are strongly anisotropic in momentum space. A detailed study should be undertaken using cluster extensions of dynamical mean-field theory but is beyond the scope of this paper.

On the experimental side, CeNiSn and CeRhSb have been established to be half-filled Kondo semimetals with a hybridization gap vanishing along a certain crystallographic axis.^{13,14,39} The CeMIn₅ compounds are candidates for Kondo metals with strongly anisotropic hybridization,⁷ but other Ce or Yb materials where a clear-cut hybridization gap in $\sigma(\omega)$ is absent may fall into this category as well. We note that first-principles calculations based on density-functional theory could, in principle, be able to determine the hybridization symmetry, but strong interaction effects can render the conclusions invalid. Recent x-ray absorption studies are promising in paving a way to an experimental determination of the required microscopic information.⁴⁰ To probe the anisotropic quasiparticle properties in the Kondo regime, high-resolution angle-resolved photoemission is the ideal tool (with the restriction that it can only be applied to quasi-2D systems). As outlined in Sec. VI, unusual behavior in the finite-temperature resistivity may also be connected to nodes in the hybridization function. Clearly, more detailed theoretical investigations of transport properties are needed. Finally, we mention that the strong-coupling pairing regime $T_c \sim T_K$ is very likely realized in the fascinating superconductor PuCoGa₅.⁴¹

Notes added. While this paper was being completed, a related paper by Ghaemi *et al.*⁴² on angle-dependent quasiparticle weights appeared. Their results for the low-temperature regime of anisotropic heavy Fermi liquids are related to ours. After submission of this paper, Shim *et al.*⁴³ published a paper on first-principles calculations for CeIrIn₅, which support the idea of a strongly momentum-dependent hybridization function.

ACKNOWLEDGMENTS

We thank F. B. Anders, K. Burch, K. Haule, J. Paglione, A. Rosch, T. Senthil, M. A. Tanatar, and V. Zlatić for discussions. This research was supported by the DFG through the SFB 608 and the Research Unit FG 960 “Quantum Phase Transitions.”

APPENDIX A: MEAN-FIELD THEORY

In this appendix, we list the expressions of Green functions required for the implementation of the mean-field theory.

1. Green functions

The Kondo lattice mean-field Hamiltonian can be rewritten in a matrix form

$$\mathcal{H}_{\text{KLM}} = \sum_{\mathbf{k}\sigma} \Psi_{\mathbf{k}}^\dagger \underbrace{\begin{pmatrix} \bar{\epsilon}_{\mathbf{k}} & b\beta_{\mathbf{k}} \\ b\beta_{\mathbf{k}} & -\lambda_0 \end{pmatrix}}_{\hat{H}_{\mathbf{k}}} \Psi_{\mathbf{k}} + \text{const}, \quad (\text{A1})$$

with $\Psi_{\mathbf{k}} = (c_{\mathbf{k}\sigma}, \tilde{f}_{\mathbf{k}\sigma})^T$. In the following, we shall denote retarded Green functions

$$\hat{G}_{AB}(z) = \int_0^\infty dt e^{izt} (-i\theta(t) \langle [\hat{A}(t), \hat{B}(0)]_+ \rangle), \quad (\text{A2})$$

as $\langle\langle \hat{A}; \hat{B} \rangle\rangle_z$. Defining the matrix propagator

$$\hat{G}(\mathbf{k}, z) = \langle\langle \hat{\Psi}_{\mathbf{k}}^\dagger; \hat{\Psi}_{\mathbf{k}} \rangle\rangle = (z - \hat{H}_{\mathbf{k}})^{-1}, \quad (\text{A3})$$

we obtain by explicit inversion,

$$\begin{aligned} \hat{G}(\mathbf{k}, z) &= \begin{pmatrix} \langle\langle c_{\mathbf{k}\sigma}^\dagger; c_{\mathbf{k}\sigma} \rangle\rangle_z & \langle\langle c_{\mathbf{k}\sigma}^\dagger; \tilde{f}_{\mathbf{k}\sigma} \rangle\rangle_z \\ \langle\langle \tilde{f}_{\mathbf{k}\sigma}; c_{\mathbf{k}\sigma} \rangle\rangle_z & \langle\langle \tilde{f}_{\mathbf{k}\sigma}; \tilde{f}_{\mathbf{k}\sigma} \rangle\rangle_z \end{pmatrix} \\ &= \frac{1}{(z - z_{1\mathbf{k}})(z - z_{2\mathbf{k}})} \begin{pmatrix} z + \lambda_0 & b\beta_{\mathbf{k}} \\ b\beta_{\mathbf{k}} & z - \bar{\epsilon}_{\mathbf{k}} \end{pmatrix}. \end{aligned} \quad (\text{A4})$$

The thermal expectation values required for the mean-field equation are obtained by summing over Matsubara frequencies; this can be done analytically, as the excitation energies [Eq. (17)] are known.

2. Green functions in the presence of a Heisenberg term

The Hamiltonian containing the additional Heisenberg term [Eq. (39)] has to be rewritten in a matrix form in analogy to Appendix A 1. The inversion of $(z - \hat{H}_{\mathbf{k}})$ provides the needed Green functions. We use the shorthand $h(z) = \prod_i (z - \bar{z}_i)$.

$$\langle\langle \tilde{f}_{\mathbf{k}\uparrow}^\dagger; \tilde{f}_{\mathbf{k}\uparrow} \rangle\rangle_z = \frac{(z - \bar{\epsilon}_{\mathbf{k}})[(z - \lambda_0)(z + \bar{\epsilon}_{\mathbf{k}}) - b^2 \gamma_{\mathbf{k}}^2]}{h(z)}, \quad (\text{A5a})$$

$$\langle\langle \tilde{f}_{-\mathbf{k}\downarrow}^\dagger; \tilde{f}_{-\mathbf{k}\downarrow} \rangle\rangle_z = \frac{(z + \bar{\epsilon}_{\mathbf{k}})[(z + \lambda_0)(z - \bar{\epsilon}_{\mathbf{k}}) - b^2 \gamma_{\mathbf{k}}^2]}{h(z)}, \quad (\text{A5b})$$

$$\langle\langle \tilde{f}_{\mathbf{k}\uparrow}^\dagger; \tilde{f}_{-\mathbf{k}\downarrow} \rangle\rangle_z = \langle\langle \tilde{f}_{-\mathbf{k}\downarrow}; \tilde{f}_{\mathbf{k}\uparrow} \rangle\rangle_z = \frac{\tilde{W}_{\mathbf{k}}(z^2 - \bar{\epsilon}_{\mathbf{k}}^2)}{h(z)}, \quad (\text{A5c})$$

$$\langle\langle c_{\mathbf{k}\uparrow}^\dagger; c_{-\mathbf{k}\downarrow}^\dagger \rangle\rangle_z = \langle\langle c_{-\mathbf{k}\downarrow}; c_{\mathbf{k}\uparrow} \rangle\rangle_z = -\frac{\tilde{W}_{\mathbf{k}} b^2 \beta_{\mathbf{k}}^2}{h(z)}, \quad (\text{A5d})$$

$$\begin{aligned} \langle\langle c_{\mathbf{k}\uparrow}^\dagger; \tilde{f}_{\mathbf{k}\uparrow} \rangle\rangle_z &= \langle\langle \tilde{f}_{\mathbf{k}\uparrow}^\dagger; c_{\mathbf{k}\uparrow} \rangle\rangle_z \\ &= \frac{b\beta_{\mathbf{k}}[(z - \lambda_0)(z + \bar{\epsilon}_{\mathbf{k}}) - b^2 \beta_{\mathbf{k}}^2]}{h(z)}, \end{aligned} \quad (\text{A5e})$$

$$\begin{aligned} \langle\langle \tilde{f}_{-\mathbf{k}\downarrow}; c_{-\mathbf{k}\downarrow}^\dagger \rangle\rangle_z &= \langle\langle c_{-\mathbf{k}\downarrow}; \tilde{f}_{-\mathbf{k}\downarrow}^\dagger \rangle\rangle_z \\ &= \frac{-b\beta_{\mathbf{k}}[(z + \lambda_0)(z - \bar{\epsilon}_{\mathbf{k}}) - b^2 \beta_{\mathbf{k}}^2]}{h(z)}, \end{aligned} \quad (\text{A5f})$$

$$\langle\langle c_{\mathbf{k}\uparrow}^\dagger; c_{\mathbf{k}\uparrow} \rangle\rangle_z = \frac{-b^2\beta_{\mathbf{k}}^2(z + \lambda_0) + (z + \bar{\epsilon}_{\mathbf{k}})(z^2 - \bar{W}_{\mathbf{k}}^2 - \lambda_0^2)}{h(z)}, \quad (\text{A5g})$$

$$\langle\langle c_{-\mathbf{k}\downarrow}; c_{-\mathbf{k}\downarrow}^\dagger \rangle\rangle_z = \frac{-b^2\beta_{\mathbf{k}}^2(z - \lambda_0) + (z - \bar{\epsilon}_{\mathbf{k}})(z^2 - \bar{W}_{\mathbf{k}}^2 - \lambda_0^2)}{h(z)}. \quad (\text{A5h})$$

APPENDIX B: EQUIVALENCE OF ANDERSON AND KONDO MEAN-FIELD THEORIES

Here, we compare the two sets of mean-field equations for the Anderson and Kondo lattice models [Eqs. (8) and (12)]. These are expected to be equivalent, once the Kondo limit is taken in the Anderson model equations. For $U \rightarrow \infty$, the Kondo coupling is $J_0 = V^2/|\epsilon_f|$. Further, the Kondo limit implies $r \rightarrow 0$, for otherwise the *effective* hybridization would diverge. The average \bar{f} occupation then becomes unity, and the \bar{f} and \tilde{f} operators are equivalent. The physical valence fluctuations in the Anderson model are projected out by $\epsilon_f \rightarrow -\infty$. In this limit, the effective \bar{f} level energy ($\epsilon_f - \lambda$) stays finite (i.e., a fraction of the bandwidth) to ensure $\sum_{\sigma} \langle \bar{f}_{\sigma}^\dagger \bar{f}_{\sigma} \rangle = 1$. Therefore, $V^2/|\lambda| \rightarrow J_0$.

With this knowledge about the limiting behaviors, the first of the Anderson model mean-field equations [Eq. (8a)] transforms like

$$\begin{aligned} rV &= \frac{1}{2\mathcal{N}} \left\langle \sum_{\mathbf{k}\sigma} \frac{V^2\beta_{\mathbf{k}}}{\lambda} (\bar{f}_{\mathbf{k}\sigma}^\dagger c_{\mathbf{k}\sigma} + c_{\mathbf{k}\sigma}^\dagger \bar{f}_{\mathbf{k}\sigma}) \right\rangle \\ &\rightarrow -\frac{J_0}{2\mathcal{N}} \left\langle \sum_{\mathbf{k}\sigma} \beta_{\mathbf{k}} (\tilde{f}_{\mathbf{k}\sigma}^\dagger c_{\mathbf{k}\sigma} + c_{\mathbf{k}\sigma}^\dagger \tilde{f}_{\mathbf{k}\sigma}) \right\rangle = b. \end{aligned} \quad (\text{B1})$$

We can see that the mean-field equations of both theories

correspond to each other, and rV and b are the effective band hybridizations in the two-band model.

APPENDIX C: OPTICAL CONDUCTIVITY

We briefly discuss the behavior of the interband optical conductivity close to the threshold energy, for the case of d -wave hybridization. In Eq. (30), the matrix elements are nonsingular near the threshold; hence, we only need to analyze the behavior of

$$\delta(\omega - \underbrace{\sqrt{(\lambda_0 + \bar{\epsilon}_{\mathbf{k}})^2 + 4b^2\beta_{\mathbf{k}}^2}}_{\Delta E(k_x, k_y)}). \quad (\text{C1})$$

A change of variables is

$$\tilde{k}_x = \frac{1}{\sqrt{2}}(k_x + k_y - 2k_0), \quad (\text{C2a})$$

$$\tilde{k}_y = \frac{1}{\sqrt{2}}(-k_x + k_y), \quad (\text{C2b})$$

where k_0 is determined by $\epsilon(k_0, k_0) = 0$. For ω near $-\lambda_0$, $\Delta E(\tilde{k}_x, \tilde{k}_y)$ can be approximated by a second-order Taylor expansion in \tilde{k}_x and \tilde{k}_y around 0. The \mathbf{k} integration is restricted to the Fermi sea because of the factor $n_F(z_{2\mathbf{k}})$. The Fermi surface can be approximated by also expanding around $\tilde{k}_x, \tilde{k}_y = 0$. Power counting in the integral then shows that the first non-vanishing contribution to the optical conductivity for a d -wave hybridization is $\propto \sqrt{\omega + \lambda_0}$.

- ¹J. Flouquet, in *Progress in Low Temperature Physics*, edited by W. Halperin (Elsevier, Amsterdam, 2005), Vol. 15.
- ²G. Stewart, *Rev. Mod. Phys.* **73**, 797 (2001); **78**, 743 (2006).
- ³H. v. Löhneysen, A. Rosch, M. Vojta, and P. Wölfle, *Rev. Mod. Phys.* **79**, 1015 (2007).
- ⁴P. Coleman, in *Handbook of Magnetism and Advanced Magnetic Materials* (Wiley, New York, in press), Vol. 1.
- ⁵A. C. Hewson, *The Kondo Problem to Heavy Fermions* (Cambridge University Press, Cambridge 1997).
- ⁶M. Sera, N. Kobayashi, T. Yoshino, K. Kobayashi, T. Takabatake, G. Nakamoto, and H. Fujii, *Phys. Rev. B* **55**, 6421 (1997).
- ⁷K. S. Burch, S. V. Dordevic, F. P. Mena, A. B. Kuzmenko, D. van der Marel, J. L. Sarrao, J. R. Jeffries, E. D. Bauer, M. B. Maple, and D. N. Basov, *Phys. Rev. B* **75**, 054523 (2007).
- ⁸L. Degiorgi, *Rev. Mod. Phys.* **71**, 687 (1999).
- ⁹S. V. Dordevic, D. N. Basov, N. R. Dilley, E. D. Bauer, and M. B. Maple, *Phys. Rev. Lett.* **86**, 684 (2001).
- ¹⁰L. Degiorgi, F. B. Anders, and G. Gruner, *Eur. Phys. J. B* **19**, 167

(2001).

- ¹¹J. N. Hancock, T. McKnew, Z. Schlesinger, J. L. Sarrao, and Z. Fisk, *Phys. Rev. Lett.* **92**, 186405 (2004).
- ¹²H. Okamura, T. Watanabe, M. Matsunami, T. Nishihara, N. Tsujii, T. Ebihara, H. Sugawara, H. Sato, Y. Onuki, Y. Isikawa, T. Takabatake, and T. Nanba, *J. Phys. Soc. Jpn.* **76**, 023703 (2007).
- ¹³H. Ikeda and K. Miyake, *J. Phys. Soc. Jpn.* **65**, 1769 (1996).
- ¹⁴J. Moreno and P. Coleman, *Phys. Rev. Lett.* **84**, 342 (2000).
- ¹⁵P. Ghaemi and T. Senthil, *Phys. Rev. B* **75**, 144412 (2007).
- ¹⁶U. Chatterjee, M. Shi, A. Kaminski, A. Kanigel, H. M. Fretwell, K. Terashima, T. Takahashi, S. Rosenkranz, Z. Z. Li, H. Raffy, A. Santander-Syro, K. Kadowaki, M. R. Norman, M. Randeria, and J. C. Campuzano, *Phys. Rev. Lett.* **96**, 107006 (2006).
- ¹⁷P. Coleman and A. M. Tsvelik, *Phys. Rev. B* **57**, 12757 (1998).
- ¹⁸N. Read and D. M. Newns, *J. Phys. C* **16**, 3273 (1983).
- ¹⁹S. Burdin, A. Georges, and D. R. Grempel, *Phys. Rev. Lett.* **85**, 1048 (2000).
- ²⁰A. Georges, G. Kotliar, W. Krauth, and M. J. Rozenberg, *Rev.*

- Mod. Phys. **68**, 13 (1996).
- ²¹C. Grenzbach, F. B. Anders, G. Czycholl, and T. Pruschke, Phys. Rev. B **74**, 195119 (2006).
- ²²Y. Haga, Y. Inada, H. Harima, K. Oikawa, M. Murakawa, H. Nakawaki, Y. Tokiwa, D. Aoki, H. Shishido, S. Ikeda, N. Watanabe, and Y. Onuki, Phys. Rev. B **63**, 060503(R) (2001).
- ²³T. Maehira, T. Hotta, K. Ueda, and A. Hasegawa, J. Phys. Soc. Jpn. **72**, 854 (2003).
- ²⁴In the mean-field approximation, the free energy also acquires a temperature dependence from the T dependence of the mean-field parameters. However, at low T , the corrections are quadratic in T , leading to specific-heat contributions $\propto T^2$, being subleading compared to $C \propto T$ from the fermionic quasiparticles (Refs. 5 and 18). Fluctuations around the mean-field solution do not change the low-temperature specific heat: amplitude fluctuations are gapped, and phase fluctuations (of r or b) do not exist, as there is no physical phase degree of freedom. [Formally, those fluctuations are gapped by the Anderson–Higgs mechanism of the compact U(1) gauge field.]
- ²⁵S. Nakatsuji, D. Pines, and Z. Fisk, Phys. Rev. Lett. **92**, 016401 (2004).
- ²⁶K. S. D. Beach, arXiv:cond-mat/0509778 (unpublished).
- ²⁷F. B. Anders (private communication).
- ²⁸G. Czycholl and H. J. Leder, Z. Phys. B: Condens. Matter **44**, 59 (1981).
- ²⁹M. A. Tanatar, J. Paglione, C. Petrovic, and L. Taillefer, Science **316**, 1320 (2007).
- ³⁰N. Read, D. M. Newns, and S. Doniach, Phys. Rev. B **30**, 3841 (1984).
- ³¹A. J. Millis and P. A. Lee, Phys. Rev. B **35**, 3394 (1987).
- ³²S. Doniach, Physica B & C **91**, 231 (1977).
- ³³T. Senthil, S. Sachdev, and M. Vojta, Phys. Rev. Lett. **90**, 216403 (2003).
- ³⁴T. Senthil, M. Vojta, and S. Sachdev, Phys. Rev. B **69**, 035111 (2004).
- ³⁵N. Read and S. Sachdev, Phys. Rev. Lett. **66**, 1773 (1991); S. Sachdev and N. Read, Int. J. Mod. Phys. B **5**, 219 (1991).
- ³⁶A decoupling of the Heisenberg interaction in the particle-hole channel is possible as well. Then, in the limit $J_H \gg T_K$, a U(1) FL* phase with gapless spinons (i.e., an RVB-like spin liquid) is realized and superconductivity does not occur (Ref. 34). As our focus here is on symmetry-broken phases competing with Kondo screening, we restrict ourselves to the particle-particle decoupling [which is selected by the Sp(2N) large- N limit].
- ³⁷M. Dzero and P. Coleman, Physica B **403**, 955 (2008).
- ³⁸The fermionic Sp(2N) mean-field theory for the Heisenberg model is known to lead to states in which the Δ fields break translational symmetry. In particular, the FL* state is unstable to dimerization. For the square lattice, it has been found that ring-exchange interactions stabilize spatially homogeneous mean-field solutions [O. I. Motrunich (private communication)]. As our interest here is in homogeneous superconducting phases, we simply impose translational invariance by hand.
- ³⁹For CeNiSn, it has been proposed that low-lying crystal-field excitations are important for a full understanding of the physical properties: K. A. Kikoin, M. N. Kiselev, A. S. Mishchenko, and A. de Visser, Phys. Rev. B **59**, 15070 (1999).
- ⁴⁰P. Hansmann, A. Severing, Z. Hu, M. W. Haverkort, C. F. Chang, S. Klein, A. Tanaka, H. H. Hsieh, H.-J. Lin, C. T. Chen, B. Fak, P. Lejay, and L. H. Tjeng, arXiv:0710.2778 (unpublished).
- ⁴¹J. L. Sarrao, L. A. Morales, J. D. Thompson, B. L. Scott, G. R. Stewart, F. Wastin, J. Rebizant, P. Boulet, E. Colineau, and G. H. Lander, Nature (London) **420**, 297 (2002).
- ⁴²P. Ghaemi, T. Senthil, and P. Coleman, arXiv:0710.2526 (unpublished).
- ⁴³J. H. Shim, K. Haule, and G. Kotliar, Science **318**, 1615 (2007).